ISSN 1674-1056
http://cpb.iphy.ac.cn
http://iopscience.iop.org/cpb
中国物理 B
Chinese Physics
中国物理
Chinese Physics B

Spectral redshift of high-order harmonics by adding a weak pulse in the falling part of the trapezoidal laser pulse

Xue-Fei Pan(潘雪飞), Jun Zhang(张军), Shuai Ben(贲帅), Tong-Tong Xu(徐彤彤), Xue-Shen Liu(刘学深)
Citation: Chin. Phys. B . 2018, 27(2): 024206. **doi:** 10.1088/1674-1056/27/2/024206

Journal homepage: http://cpb.iphy.ac.cn; http://iopscience.iop.org/cpb

What follows is a list of articles you may be interested in

Laser phase effect on asymmetric harmonic distribution in H_2^+

Li-Qiang Feng(冯立强), Wen-Liang Li(李文亮), Hui Liu(刘辉)
Chin. Phys. B . 2017, 26(4): 044206. **doi:** 10.1088/1674-1056/26/4/044206

Optimization of multi-color laser waveform for high-order harmonic generation

Cheng Jin(金成), C D Lin(林启东)
Chin. Phys. B . 2016, 25(9): 094213. **doi:** 10.1088/1674-1056/25/9/094213

Multi-level effects in the high-order harmonic generation driven by intense frequency-comb laser fields

Zhao Di, Jiang Chen-Wei, Li Fu-Li
Chin. Phys. B . 2015, 24(7): 074205. **doi:** 10.1088/1674-1056/24/7/074205

Attosecond pulse generation from two-electron harmonic emission spectrum

Feng Li-Qiang, Liu Hang
Chin. Phys. B . 2015, 24(3): 034206. **doi:** 10.1088/1674-1056/24/3/034206

Generation of the wavelength-tunable XUV pulse using the two-color and three-color infrared pulses

Feng Li-Qiang, Liu Hang, Liu Xing-Jiang
Chin. Phys. B . 2014, 23(6): 064206. **doi:** 10.1088/1674-1056/23/6/064206

Spectral redshift of high-order harmonics by adding a weak pulse in the falling part of the trapezoidal laser pulse*

Xue-Fei Pan(潘雪飞), Jun Zhang(张军), Shuai Ben(贲帅),
Tong-Tong Xu(徐彤彤), and Xue-Shen Liu(刘学深)†

Institute of Atomic and Molecular Physics, Jilin University, Changchun 130012, *China*

(Received 17 September 2017; revised manuscript received 13 October 2017; published online 5 January 2018)

We investigate the spectral redshift of high-order harmonics of the H_2^+ (D_2^+) molecule by numerically solving the non-Born–Oppenheimer time-dependent Schrödinger equation (TDSE). The results show that the spectral redshift of high-order harmonics can be observed by adding a weak pulse in the falling part of the trapezoidal laser pulses. Comparing with the H_2^+ molecule, the shift of high-order harmonic generation (HHG) spectrum for the D_2^+ molecule is more obvious. We employ the spatial distribution in HHG and time-frequency analysis to illustrate the physical mechanism of the spectral redshift of high-order harmonics.

Keywords: high-order harmonic generation, spectral redshift, trapezoidal laser pulse, spatial distribution

PACS: 42.65.Ky, 32.80.Rm, 78.67.Bf **DOI:** 10.1088/1674-1056/27/2/024206

1. Introduction

Attosecond pulse as a tool to trace the electron motion is gaining extensive attention. Usually, the HHG is one of the effective techniques to generate the attosecond pulses.[1–3] For the atoms[4] and molecules,[5] the HHG has been widely studied in the past few decades. Corkum[6] presented the three step model to interpret the process of the HHG. The electron leaves its parent core by tunneling, then it is accelerated and moves away from its parent core. When the laser field changes its direction, the electron returns to the parent core followed by harmonic emission.

For molecular HHG, the nuclear motion affects the ionization and recombination process.[7–9] Lein[10] investigated the HHG, and presented a method on reconstructing the nuclear motion to measure the attosecond pulse. Zhang *et al.*[11] illustrated the HHG of the H_2^+ molecule, and presented the spatial distribution. Miao *et al.*[12] presented the multichannel HHG from the asymmetric molecule, and found that the recombination channels from different electronic states make different contributions to HHG. By considering nuclear motion, Bian *et al.*[13] investigated the redshift of the HHG spectrum, and confirmed that the dissociation of molecules lead to an obvious redshift in frequency modulation (FM) with intercycle dynamics in harmonic spectra. Du *et al.*[14] illustrated the nonadiabatic spectral redshift, and the result shows that the spectral redshift can be observed by adjusting the laser pulse of the falling part.

With a detailed analysis of these nonadiabatic redshifts, Silva *et al.*[15] evaluated that the even-order harmonics generation can be controlled by pulse duration. For the even-order harmonics generation, the electron localization and the molecular dissociation are investigated. The localization of the electronic wave packet in the process of HHG with different pulses envelpoe was demonstrated.[16] Morales *et al.*[17] investigated the electron localization on the HHG, and found that the even-order harmonic generation can be observed. The shift of HHG spectrum with variational initial vibrational states was reported,[18] the redshift and blueshift of HHG can be controlled by changing the initial vibrational state, and the shift of the HHG spectrum can be observed by increasing the nuclear distance R.

In this paper, we investigate the redshift of high-order harmonic under combined laser pulse. The spatial distribution in HHG and time-frequency analysis are used to illustrate the physical mechanism of the spectral redshift of high-order harmonics. We also investigate the HHG spectra of the D_2^+ molecule.

2. Theoretical model

We investigate the spectral redshift of HHG by numerically solving the TDSE of the one-dimensional H_2^+ molecule within the non-Born–Oppenheimer approximation. The initial wave function is obtained under a sine discrete variable representation (DVR),[19] the initial electronic state is the ground state with the lowest energy, the initial vibrational state is the vibrational ground state $v = 0$. In the dipole approximation and the length gauge, the time-dependent Schrödinger equation reads (atomic units are used throughout, unless otherwise stated)

$$\mathrm{i}\frac{\partial}{\partial t}\Psi(z,R,t) = H(z,R,t)\Psi(z,R,t)$$

*Project supported by the National Natural Science Foundation of China (Grant No. 61575077) and the Graduate Innovation Fund of Jilin University (Grant No. 2017107).

†Corresponding author. E-mail: liuxs@jlu.edu.cn

© 2018 Chinese Physical Society and IOP Publishing Ltd

$$= [T_{\rm R} + T_{\rm e} + V_C(z,R) + V_I(z,t)]\Psi(z,R,t), \quad (1)$$

where $T_{\rm R} = -(1/m_{\rm p})(\partial^2/\partial R^2)$ and

$$T_{\rm e} = -(2m_{\rm p} + m_{\rm e})/(4m_{\rm p}m_{\rm e})(\partial^2/\partial z^2)$$

are the kinetic energy of the nuclei and the electron. $m_{\rm e}$ and $m_{\rm p}$ are the masses of the electron and proton ($m_{\rm e} = 1$ a.u. and $m_{\rm p} = 1836$ a.u.), respectively. The $V_{\rm C}$ is the soft-core Coulomb potential for the H_2^+ molecule,

$$V_{\rm C}(z,R) = \frac{1}{R} - \frac{1}{\sqrt{(z-R/2)^2+a}} - \frac{1}{\sqrt{(z+R/2)^2+b}}, \quad (2)$$

$V_{\rm I}$ is the laser-molecule interaction term which has the form

$$V_{\rm I}(z,t) = \left(1 + \frac{m_{\rm e}}{2m_{\rm p}+m_{\rm e}}\right) zE(t), \quad (3)$$

where z is the electronic coordinate, and it is taken to be along the internuclear axis. R is the internuclear distance. The soft-core parameters are adopted to $a = b = 1$, and the equilibrium internuclear distance is 2.6 a.u., the ionization energy is -21.2 eV. The time-dependent wave functions are obtained by using the second-order splitting-operator approach.[20] All the calculations have been performed using the attosecond resolution quantum dynamics program LZH-DICP.[21–23] The grid sizes of the R axis and z axis are selected as 30 a.u. and 200 a.u., respectively. The spatial steps are $\Delta z = 2\Delta R = 0.2$ a.u., the time step is 0.2 a.u. The absorbing positions of the mask function are 25 a.u. from the end of the electronic coordinate.[22,24]

According to the Ehrenfest theorem,[25,26] the dipole acceleration can be written by

$$a(t) = \frac{{\rm d}^2}{{\rm d}t^2}\langle\Psi(z,R,t)|z|\Psi(z,R,t)\rangle$$

$$= -\langle\Psi(z,R,t)\left|\frac{{\rm d}V_C(z,R)}{{\rm d}z}\right. + \left(1 + \frac{m_{\rm e}}{2m_{\rm p}+m_{\rm e}}\right)E(t)|\Psi(z,R,t)\rangle. \quad (4)$$

The HHG spectrum can be obtained by means of Fourier transformation.

$$P_{\rm a}(\omega) \sim \left|\frac{1}{T}\int_0^T a(t)\,{\rm e}^{-{\rm i}\omega t}\,{\rm d}t\right|^2. \quad (5)$$

In order to investigate the spatial symmetry of the system, we investigate the spatial distribution in HHG for the H_2^+ molecule in an intense laser field, the dipole acceleration distribution in each electronic coordinate z and internuclear distance R can be written as[11,27]

$$d_{\rm A}(z,t) = -\int_0^R \Psi^*(z,R,t)\left[\frac{{\rm d}V_C(z,R)}{{\rm d}z} + \left(1 + \frac{m_{\rm e}}{2m_{\rm p}+m_{\rm e}}\right)E(t)\right]\Psi(z,R,t)\,{\rm d}R, \quad (6)$$

$$d_{\rm A}(R,t) = -\int_{-\infty}^{\infty} \Psi^*(z,R,t)\left[\frac{{\rm d}V_C(z,R)}{{\rm d}R} + \left(1 + \frac{m_{\rm e}}{2m_{\rm p}+m_{\rm e}}\right)E(t)\right]\Psi(z,R,t)\,{\rm d}z. \quad (7)$$

3. Results and discussion

We investigate the HHG of the $H_2^+(D_2^+)$ molecule with the combination of the trapezoidal laser and a weak laser pulse of the $\sin^2$ envelope

$$E(t) = \begin{cases} E_1 f_1(t)\cos(\omega t), & t < 4 \text{ o.c.}, \\ E_1 f_1(t)\cos(\omega t) + E_2 f_2(t - t_{\rm delay})\cos\left(\omega(t - t_{\rm delay}) - \pi\right) & t \geq 4 \text{ o.c.}, \end{cases} \quad (8)$$

where ω denotes the frequency of two laser pulses, E_1 and E_2 are the peak amplitude of the trapezoidal laser pulse respectively, and weak laser pulse, and $f_1(t)$ is the pulse envelope of the trapezoidal laser pulse. The trapezoidal laser pulse has seven optical cycles (o.c.), the duration of the rising and falling parts are both two cycles. $f_2(t) = \sin(\pi t/\tau)^2$ is the pulse envelope of the weak laser pulse. $\tau = 3T_0$ is the total duration of the weak laser pulse, where T_0 is the optical cycle (o.c.) of the fundamental pulse. $t_{\rm delay} = 4T_0$ is the time delay between the two pulses. We choose the wavelength $\lambda = 800$ nm and the corresponding intensities of the two pulses are $I_1 = 5 \times 10^{14}$ W/cm^2 and $I_2 = 3 \times 10^{13}$ W/cm^2.

Figure 1 shows the trapezoidal laser pulse (dashed red curve), the combined laser pulse (solid blue curve) and the weak laser pulse of the $\sin^2$ envelope (dotted green curve). We can see that the peak intensity of the weak laser pulse of the $\sin^2$ envelope reaches its negative maximum, when the peak intensity of the trapezoidal laser reaches its positive maximum, after 4 optical cycles. Thus, the decrease of the effective amplitude of the combined laser pulse in the falling part of the fundamental pulse can be well achieved.

The HHG spectra of H_2^+ and D_2^+ obtained under trapezoidal laser pulse and combined laser pulse are shown in Fig. 2. The intensity of harmonics for the H_2^+ (D_2^+) molecule in the combined laser pulse are shifted down by 2 orders (4 orders) for clarity, and harmonic orders between 1st and 33rd, 35th and 65th, and 67th and 97th are separately shown in Fig. 2(a), Fig. 2(b), and Fig. 2(c) for a better visualization. We know that the nuclear motion will lead to the frequency modulation of intercycle dynamics in MHOHG which results

in the redshift. This phenomenon has also been mentioned in Ref. [13]. In Fig. 2(a), the harmonic spectra show that odd harmonics are dominant for the trapezoidal laser pulse and combined laser pulse; small redshifts in odd orders can be ignored. Meanwhile, we can see that the high-order harmonic spectrum of the $D_2{}^+$ is similar to that of the $H_2{}^+$ for the trapezoidal laser pulse as shown in Fig. 2(b), and the odd harmonic with small redshift is generated. While for the combined laser pulses, the HHG spectra exhibit a larger redshift from odd harmonics compared with the trapezoidal laser pulse. Meanwhile, we can see that the redshift of the spectra for the $D_2{}^+$ molecule is larger than the $H_2{}^+$ molecule. When the weak pulse is added to the falling part of the trapezoidal laser pulse, the change of the falling parts of the laser pulse is faster. We know that the nuclear motion of the $D_2{}^+$ molecule is slower than that of the $H_2{}^+$ molecule in the same laser pulse, the peak of the harmonic signals from the $H_2{}^+$ molecule appears earlier (we give the detailed explanations in the next part of this article by the time-frequency distribution of the HHG spectra). Compared with the $H_2{}^+$ molecule, the effective intensity of the HHG for the $D_2{}^+$ molecule has a rapid change,[13] which results in a more obvious redshift. For the harmonic order between the 67th and 97th as shown in Fig. 2(c), the harmonic order has a sharp cutoff at about the 83rd. The high-order harmonic spectrum of $H_2{}^+$ and $D_2{}^+$ molecule show that odd harmonics with small redshift are dominant in the trapezoidal laser pulse. Compared with the harmonic orders between the 35th and 65th in Fig. 2(b), the spectral redshift of high-order harmonics become weak and odd harmonic with small redshif are dominant for the $H_2{}^+$ and $D_2{}^+$ molecules driven by combined laser pulse.

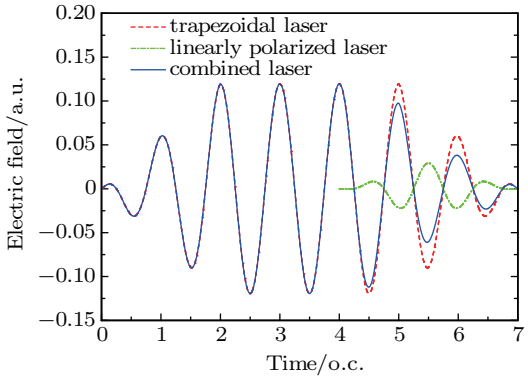


Fig. 1. (color online) The electric fields of the trapezoidal laser pulse (dashed red curve), the combined laser pulse (solid blue curve), and the weak laser pulse of the $\sin^2$ envelope (dotted green curve).

The time frequency distribution of the HHG spectra is obtained by a wavelet analysis:[28,29] $A(t_0,\omega) = \int_{-\infty}^{\infty} f(t)\, w_{t_0,\omega}(t)\, \mathrm{d}t$, with the wavelet kernel $w_{t_0,\omega}(t) = \sqrt{\omega} W[\omega(t-t_0)]$. The mother wavelet which we use is a Morlet wavelet: $W(x) = (1/\sqrt{\sigma})\, \mathrm{e}^{\mathrm{i}x}\, \mathrm{e}^{-x^2/2\tau^2}$ ($\sigma = 15$ a.u.).

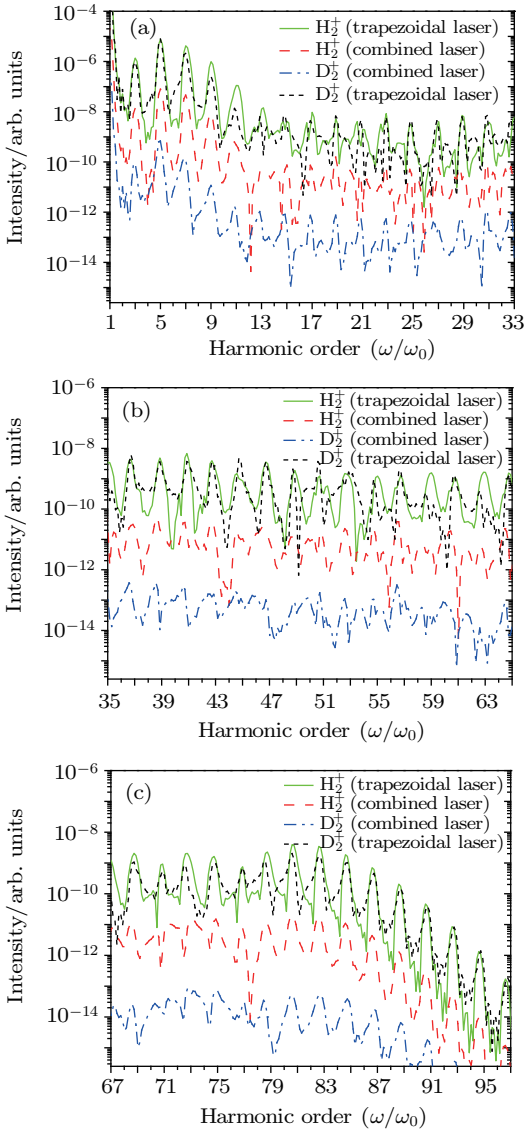


Fig. 2. (color online) The HHG spectrum produced from the $H_2{}^+$ ($D_2{}^+$) molecule in the trapezoidal laser pulse and the $H_2{}^+$ ($D_2{}^+$) molecule in the combined laser pulse. The intensities of harmonics for the $H_2{}^+$ ($D_2{}^+$) molecule in the combined laser pulse are shifted down by 2 orders (4 orders) for clarity. The harmonic orders between the 1st and 33rd, 35th and 65th, and 67th and 97th are separately shown in Fig. 2(a), Fig. 2(b), and Fig. 2(c) for a better visualization.

In Fig. 3(a) to Fig. 3(c) we present the time-frequency distribution of HHG spectra. Figure 3(a) shows the time-frequency distribution from the $H_2{}^+$ molecule driven by the trapezoidal laser pulse. We can see that there is almost no contribution to HHG in the rising part of the laser pulse between 0–2 laser cycles. The main contribution to HHG comes from 2–5 laser cycles, and the contribution from the falling part of the laser pulse plays less of a role in comparison with the region between 2–5 laser cycles. Figures 3(b) and 3(c) show the time-frequency of HHG from the $H_2{}^+$ and $D_2{}^+$ molecules driven by the combined laser pulse. From the harmonic order between 25th and 50th as shown in the dashed rectangular box in Fig. 3, we can see that the main emission time of the harmonic is delayed and the peak of the harmonic signals shifts to the right in the combined laser pulse as shown in Fig. 3(b)

compared with that in the trapezoidal laser pulse as shown in Fig. 3(a). Moreover, the intensity of harmonic in the falling part of the laser pulse between 5–7 laser cycles is increased as indicated by the arrow; the main harmonic signals gradually shift to the falling part of the laser pulse. Thus the redshift is observed. In Fig. 3(c) we can see that the main harmonic signals in 5–7 laser cycles are much stronger compared with that from H_2^+ as shown in Fig. 3(b) as indicated by the arrow, the shift of the peak of the harmonic signals is more obvious, the redshift is obviously observed. The spectral redshift of high-order harmonic generation can be interpreted through the three-step model. The electron is ionized through tunneling or multiphoton from the ground state, then it is accelerated in the external laser field, and finally recombines with the parent ion followed by harmonic emission. When the second pulse is added, the effective amplitude on the falling part of the laser cycle is decreased. When the electrons return to the ground state, the electron will have a phase shift relative to the field, which results in the spectra redshift.[14]

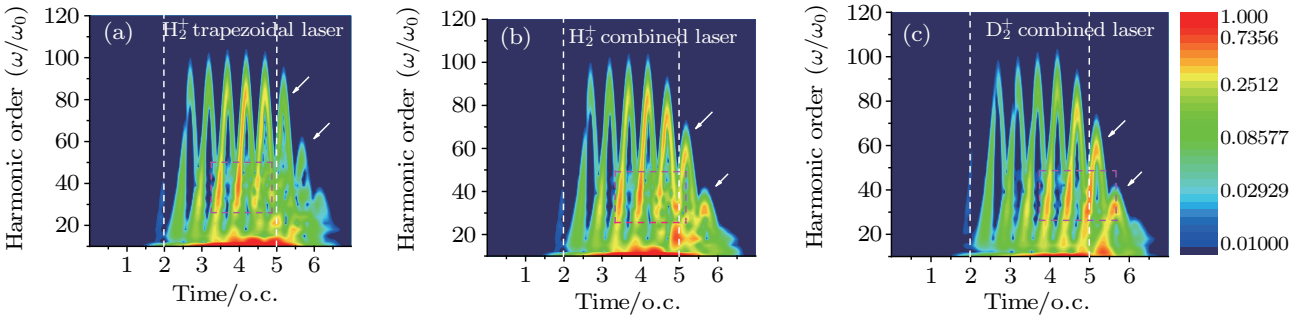


Fig. 3. (color online) The time-frequency distribution of the HHG spectra from (a) H_2^+ molecule driven by the trapezoidal laser pulse, (b) H_2^+ molecule driven by the combined laser pulse, and (c) D_2^+ molecule driven by the combined laser pulse.

Figure 4(a) shows the spatial distribution of the H_2^+ molecule driven by the trapezoidal laser pulse, we can see that the odd harmonics are dominant. Figures 4(b) and 4(c) show the spatial distributions of the H_2^+ molecule and the D_2^+ molecule driven by the combined laser pulse. From Fig. 4(a) we can see that only an odd harmonic is generated. From Fig. 4(b), we can see that, for $R < 3.5$ a.u., only an odd harmonic is generated; for $R > 3.5$ a.u., the small redshifts in odd orders can be observed. When the nuclear distance R is increased, the shift in odd orders is more obvious. From Fig. 4(c) we can see that the HHG spectra exhibit a larger redshift from odd harmonics for the gradually increasing nuclear distance R, which means that the shift of HHG spectrum of the D_2^+ molecule as shown in Fig. 4(c) is more obvious than that of the H_2^+ molecule as shown in Fig. 4(b). During the first few cycles for the fundamental frequency of 800 nm, the intensity of intense laser field is not enough to make the electron significantly ionized, the electron is oscillatory between $1s\sigma_g$ and $2p\sigma_u$ state. When the nuclear packet reaches ~ 3.5 a.u., the energy difference between the $1s\sigma_g$ and $2p\sigma_u$ becomes resonance with absorption of three photons. A coherent superposition of the $1s\sigma_g$ and $2p\sigma_u$ state is created, which leads to electron localization. The electron density is asymmetric, and the spectral redshift of high-order harmonics are observed.[15]

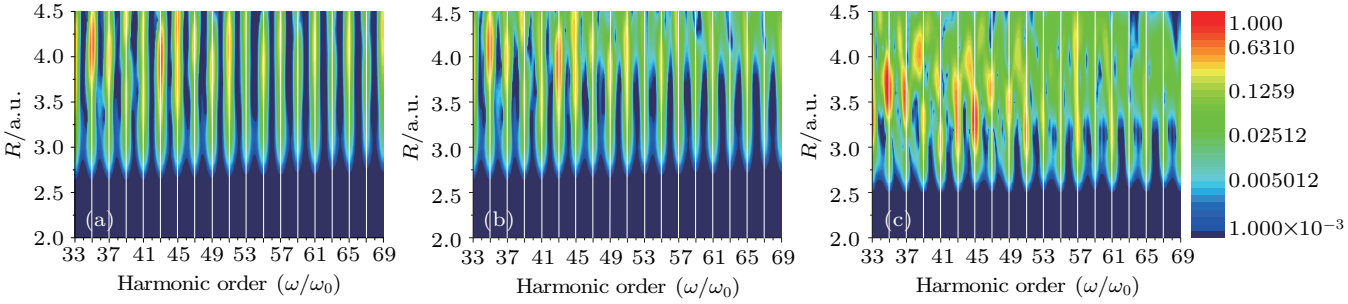


Fig. 4. (color online) Spatial distribution in HHG spectra as a function of the internuclear distance R and harmonic order, (a) H_2^+ molecule driven by the trapezoidal laser pulse, (b) H_2^+ molecule driven by the combined laser pulse, and (c) D_2^+ molecule driven by the combined laser pulse.

To further investigate the physical mechanism of the spectral redshift of high-order harmonics, the spatial distribution of the HHG spectra as a function of the electronic coordinate z and the harmonic order between the 33rd and 69th is shown in Fig. 5. Figure 5(a) shows the spatial distribution in HHG spectra of the H_2^+ molecule for the trapezoidal laser pulse, which seems to be symmetric with respect to $z = 0$. Figures 5(b) and 5(c) show the spatial distributions of the H_2^+ and D_2^+ molecules driven by the combined laser field, the HHG symmetry with respect to $z = 0$ is broken. For the harmonic order between the 52nd and 57th as shown in Fig. 5(b), the contribution from the nucleus at $z < 0$ is larger than that at $z > 0$. In addition, from the harmonic order

between the 63rd and 66th we can see that the contribution from the nucleus at $z > 0$ is larger than that at $z < 0$. Meanwhile, from the harmonic order between the 54th and 59th as shown in Fig. 5(c), the contribution from the nucleus at $z < 0$ is larger than that at $z > 0$. We can see that the electron localization on the nuclei can be controlled by synthesizing a weak laser pulse of the $\sin^2$ envelope to the trapezoidal laser pulse. The electronic wave packet is localized on the surrounding of a nucleus, and has a larger probability of recombining with the nucleus.[30] Meanwhile, the spatial distribution of the HHG spectra at $z > 0$ and $z < 0$ is asymmetric, which leads to the spectral redshift of high-order harmonics.

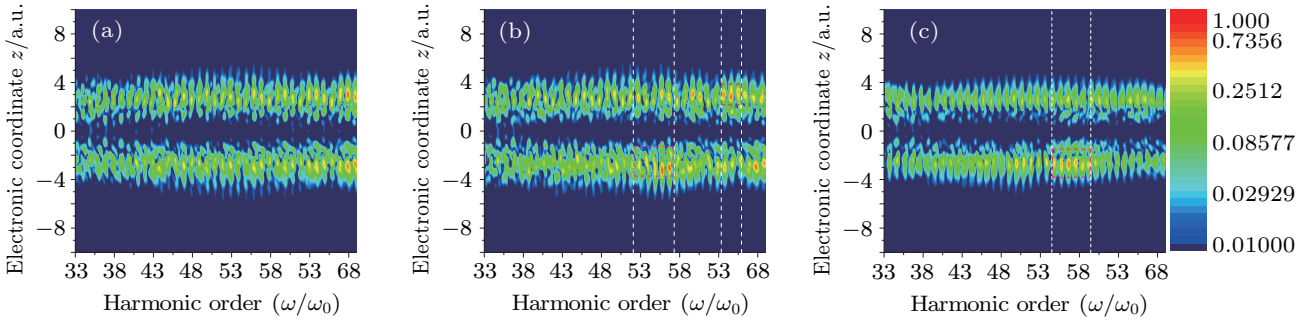


Fig. 5. (color online) Spatial distribution in HHG spectra as a function of the electronic coordinate and harmonic order between the 33rd and 69th, (a) H_2^+ molecule driven by the trapezoidal laser pulse, (b) H_2^+ molecule driven by the combined laser pulse, and (c) D_2^+ molecule driven by the combined laser pulse.

For the trapezoidal laser pulse, we can see that the main contribution to HHG comes from 2–5 laser cycles, and the falling part of the laser pulse plays less of a role from the time–frequency analysis as shown in Fig. 3(a). Thus, odd harmonics are dominant and the small redshifts in odd orders can be ignored. The spatial distribution of the HHG spectra seems to be symmetric with respect to $z = 0$ as shown in Fig. 5(a).

The blueshift and redshift of harmonic occur due to the change of the rising and falling parts of the laser pulse, respectively. On the rising part of the laser pulse, $\partial I(t)/\partial t > 0$ results in a blueshift in HHG, on the falling part of the laser pulse, $\partial I(t)/\partial t < 0$ results in redshift.[13,14] The spectra redshift will arise due to the rapid change on the falling edge of the laser pulse. We can adjust the value of $|\partial I(t)/\partial t|$ to generate the spectra redshift of high-order harmonics. When the second pulse is added, the weak pulse leads to the electron localization. The aim of adding the weak pulse is to control the electron localization on the nuclei, which will make a different contribution to HHG from the two nuclei. In this case, we can observe the asymmetric spatial distribution of the HHG spectra at $z > 0$ and $z < 0$ as shown in Fig. 5, which leads to the spectral redshift of high-order harmonics.

In order to further illustrate the asymmetry of the HHG with respect to the $z = 0$ for the combined laser pulse, we define an asymmetric parameter

$$A = (P_{a_{z>0}}(\omega) - P_{a_{z<0}}(\omega))/(P_{a_{z>0}}(\omega) + P_{a_{z<0}}(\omega)),$$

where $P_{a_{z>0}}(\omega)$ and $P_{a_{z<0}}(\omega))$ are the HHG spectrum obtained by means of Fourier transformation of the dipole acceleration.[11,31]

$$P_{a_{z>0}}(\omega) \sim \left| \frac{1}{T} \int_0^T a_{z>0}(t)\, \mathrm{e}^{-\mathrm{i}\omega t}\, \mathrm{d}t \right|^2, \tag{9}$$

$$P_{a_{z<0}}(\omega) \sim \left| \frac{1}{T} \int_0^T a_{z<0}(t)\, \mathrm{e}^{-\mathrm{i}\omega t}\, \mathrm{d}t \right|^2, \tag{10}$$

where

$$a_{z>0}(t) = -\int_0^{\infty} \int_0^{R} \Psi^*(z,R,t) \left[\frac{\mathrm{d}V_C(z,R)}{\mathrm{d}z} \left(1 + \frac{m_\mathrm{e}}{2m_\mathrm{p} + m_\mathrm{e}} \right) E(t) \right] \Psi(z,R,t)\, \mathrm{d}R\mathrm{d}z, \tag{11}$$

$$a_{z<0}(t) = -\int_{-\infty}^{0} \int_0^{R} \Psi^*(z,R,t) \left[\frac{\mathrm{d}V_C(z,R)}{\mathrm{d}z} + \left(1 + \frac{m_\mathrm{e}}{2m_\mathrm{p} + m_\mathrm{e}} \right) E(t) \right] \Psi(z,R,t)\, \mathrm{d}R\mathrm{d}z. \tag{12}$$

Figure 6 shows the asymmetric parameter A as a function of the harmonic order. Figure 6(a) shows the asymmetric parameter of the H_2^+ molecule for the trapezoidal laser pulse. The HHG spectra seem to be symmetric with respect to $z = 0$, which is in agreement with the spatial distribution in HHG as shown in Fig. 5(a). Figures 6(b) and 6(c) show the asymmetric parameter of H_2^+ and D_2^+ molecules for the combined laser pulse, the HHG symmetry with respect to $z = 0$ is broken. For the harmonic order between the 52nd and 57th as shown in Fig. 6(b), the contribution from the nucleus at $z < 0$ is larger than that at $z > 0$. For the harmonic order between the 63rd and 66th as shown in Fig. 6(b), the contribution from the nucleus at $z > 0$ is larger than that at $z < 0$, which is in agreement with the spatial distribution of the HHG spectra shown in Fig. 5(b). Meanwhile from the harmonic order between the 54th and 59th in Fig. 6(c), the contribution from the nucleus at $z < 0$ is larger than that at $z > 0$, which is in

agreement with the spatial distribution of the HHG spectra shown in Fig. 5(c). We can see that the HHG symmetry with respect to $z = 0$ is broken, which leads to the spectral redshift of high-order harmonics.

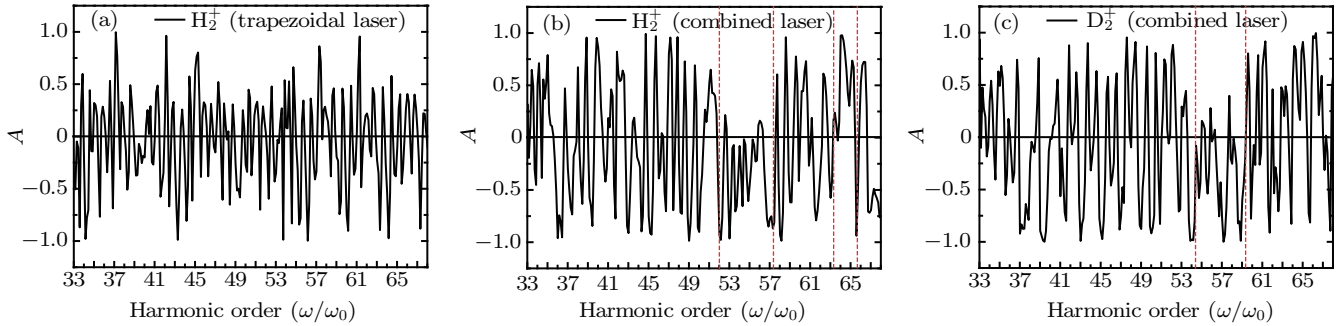


Fig. 6. (color online) The asymmetric parameter A of the (a) H_2^+ molecule in the trapezoidal laser pulse, (b) H_2^+ molecule in the combined laser pulse, and (c) D_2^+ molecule in the combined laser pulse.

4. Conclusions

In this paper, we have numerically solved the TDSE of one-dimensional H_2^+ and its isotope within the non-Born–Oppenheimer approximation to investigate the spectral redshift in HHG. The results show that the spectral redshift of high-order harmonics can be observed by adding a weak pulse in the falling part of the trapezoidal laser pulses. Meanwhile, the main emission time of the harmonic is delayed and the peak of the harmonic signals shifts to the right in the combined laser pulse compared with that in the trapezoidal laser pulse. The physical mechanism of the spectral redshift of high-order harmonics can be well understood by the spatial distribution in HHG and time-frequency analysis. The spatial distribution of H_2^+ and D_2^+ molecules driven by the combined laser field from the harmonic order between the 33rd and 69th shows that the HHG symmetry with respect to $z = 0$ is broken compared with the trapezoidal laser pulse, which results in the spectral redshift of high-order harmonics.

Acknowledgments

The authors sincerely thank Prof. Keli Han and Dr. Ruifeng Lu for providing us with the LZH-DICP code.

References

[1] Edwards M R and Mikhailova J M 2016 *Phys. Rev. A* **93** 023836
[2] Chou Y, Li P C, Ho T S and Chu S I 2015 *Phys. Rev. A* **91** 063408
[3] Du H, Pan X F, Liu H F, Zhang H D, Zhang J, Guo J and Liu X S 2016 *Chin. Phys. B* **25** 093202
[4] Ciappina M F, Hernández J A P, Shaaran T, Biegert J, Quidant R and Lewenstein M 2012 *Phys. Rev. A* **86** 023413
[5] Telnov D A, Heslar J and Chu S I 2014 *Phys. Rev. A* **90** 063412
[6] Corkum P B 1993 *Phys. Rev. Lett.* **71** 1994
[7] Yuan X L, Wei P F, Liu C D, Ge X C, Zheng Y H, Zeng Z N and Li R X 2016 *Opt. Express* **24** 8194
[8] Li W Y, Yu S J, Wang S and Chen Y J 2016 *Phys. Rev. A* **94** 053407
[9] Feng L Q, Li W L and Liu H 2017 *Chin. Phys. B* **26** 044206
[10] Lein M 2005 *Phys. Rev. Lett.* **94** 053004
[11] Zhang J, Ge X L, Wang T, Xu T T, Guo J and Liu X S 2015 *Phys. Rev. A* **92** 013418
[12] Miao X Y and Zhang C P 2014 *Phys. Rev. A* **89** 033410
[13] Bian X B and Bandrauk A D 2014 *Phys. Rev. Lett.* **113** 193901
[14] Du H C, Xue S, Wang H Q, Zhang Z L and Hu B T 2015 *Phys. Rev. A* **91** 063844
[15] Silva R E F, Rivière P, Morales F, Smirnova O, Ivanov M and Martín F 2016 *Sci. Rep.* **6** 32653
[16] Ahmadi H, Vafaee M and Maghari A 2016 *Phys. Rev. A* **94** 033415
[17] Morales F, Rivière P, Richter M, Gubaydullin A, Ivanov M, Smirnova O and Martín F 2014 *J. Phys. B: At. Mol. Opt. Phys.* **47** 204015
[18] Zhang J, Pan X F, Xu T T and Liu X S 2017 *Laser Phys. Lett.* **14** 055302
[19] Sharafeddin O and Zhang J Z H 1993 *Chem. Phys. Lett.* **204** 190
[20] Feit M D and Fleck J A Jr 1983 *J. Chem. Phys.* **78** 301
[21] Lu R F, He H X, Guo Y H and Han K L 2009 *J. Phys. B: At. Mol. Opt. Phys.* **42** 225601
[22] Lu R F, Zhang P Y and Han K L 2008 *Phys. Rev. E* **77** 066701
[23] Hu J, Han K L and He G Z 2005 *Phys. Rev. Lett.* **95** 123001
[24] Miao X Y and Zhang C P 2014 *Laser Phys. Lett.* **11** 115301
[25] Burnett K, Reed V C, Cooper J and Knight P L 1992 *Phys. Rev. A* **45** 3347
[26] Bian X B and Bandrauk A D 2010 *Phys. Rev. Lett.* **105** 093903
[27] Lein M, Hay N, Velotta R, Marangos J P and Knight P L 2002 *Phys. Rev. Lett.* **88** 183903
[28] Antoine P, Piraux B and Maquet A 1995 *Phys. Rev. A* **51** R1750
[29] Chandre C, Wiggins S and Uzer T 2003 *Physica D* **181** 171
[30] Liu K L, Zhang Q B and Lu P X 2012 *Phys. Rev. A* **86** 033410.
[31] Wang J, Chen G, Guo F M, Li S Y, Chen J G and Yang Y J 2013 *Chin. Phys. B* **22** 033203